Assessment of GPS Signal Multipath Interference

Sung H. Byun, George A. Hajj, and Lawrence E. Young
Jet Propulsion Laboratory, California Institute of Technology

BIOGRAPHY

Sung Byun received his Ph.D degree in Aerospace Engineering and Engineering Mechanics from the University of Texas at Austin. He is currently working at the Tracking Systems and Applications Section at Jet Propulsion Laboratory. His main research is focused on low earth satellite orbit determination using GPS and other scientific applications of GPS.

George Hajj received his Ph.D in physics from Rice University. He is a principal member of the technical staff at the Jet Propulsion Laboratory. His research interests include the use of GPS-LEO occultations for remote sensing of the Earth's atmosphere, ionospheric tomography and ionospheric data assimilation.

Dr. Larry Young has developed radiometric technology at Caltech's Jet Propulsion Laboratory since 1978, currently supervising a group developing high precision GPS receivers application. Specific areas of group research include digital GPS receivers, multipath mitigation, sub-nanosecond clock synchronization, and sub-cm formation flying. Ongoing work includes investigating GPS occulations and surface reflections as remote sensing tools. Larry received a Ph.D in Nuclear Physics from SUNY at Stony Brook in 1975, and a B.A. in Physics from Johns Hopkins in 1970. He served on the National Research Council's 1995 Committee on the Future of GPS, and is currently (2000/2002) Space Representative to the Institute of Navigation Council.

ABSTRACT

Multipath is the phenomenon where a signal arrives at an antenna via several paths due to signal reflection and diffraction. These paths are superimposed on the direct signal at the antenna with a different phase and amplitude, and can result in significant ranging errors.

A multipath simulator, MUSTARD (MUltipath Simulator Taking into Account Reflection and Diffraction), has been developed at the Jet Propulsion Laboratory. In essence, the simulator traces the signal as it is transmitted by the GPS satellite to a user's receiver accounting for all possible paths the signal can take by reflecting or diffracting from the surrounding surfaces. The simulator uses simplified model of the real multipath environment. In modeling the reflection and diffraction from each surface, the Geometric Theory of Diffraction (GTD) is used. The multipath signals are then added to the direct signal after accounting for the gain of the receiving antenna. The receiver's tracking loop is then simulated and then range and phase multipath error are estimated.

The multipath simulator can be used in the initial design phase of an experiment to identify hazardous environmental configuration that can cause severe multipath. By using the simulator we can also assess the upper limits on the antenna backlobes gains, and be able to determine the ideal antenna location, height, and orientation to minimize the multipath error within a given environment. Once the optimal geometric configuration is determined, it can provide a realistic quantitative estimate of multipath errors on GPS data. This in turn can provide means of testing different ways of analyzing the data to reduce the solution errors from multipath. With a given environment, this simulator is a valuable tool to quantitatively assess the multipath effect on the GPS measurement.

INTRODUCTION

The Global Positioning System (GPS) has been shown to be capable of supporting a wide variety of applications. Current baseline solutions accuracies using the GPS is 1-2 parts in 10^9, while those of orbit positioning are of the order of few parts in 10^9. A wide range of techniques have been developed over the past fifteen years that must be used in order to achieve such accuracies. Data accuracies are limited by instrumental thermal noise, tropospheric effects, higher order ionospheric effects, and multipath. Advanced receiver's instrumental noise is now reaching an RMS of 10 cm for range (P-code) and 0.1 mm for range-rate (phase) after one second averaging. The tropospheric effect can be modeled to the cm level while higher order ionospheric effects, under normal conditions, are expected to be less than 1 cm (Bassiri and Hajj 1993).

Differential GPS can greatly reduce common errors resulting from atmospheric delay, GPS orbit, and GPS and/or receiver clocks. However, the GPS multipath errors can not be removed by differential approach since multipath is a highly localized phenomenon. Thus, one of the major error contributors to GPS positioning application can be multipath.

Multipath is the phenomenon where a signal arrives at an antenna via several paths due to signal reflection and diffraction. Multipath error is scaled according to wavelength and is generally therefore nearly 100 times larger for P-code than carrier phase. Instantaneous multipath error can be as large as few meters for P-code and few centimeters for carrier phase. Thus, in situations where instantaneous range and phase data, or data averaged over small time intervals are needed, multipath becomes a dominant source of error to the measurement.

In addition to contributing to positioning error, multipath can cause serious problems on a host of other GPS derived applications. Examples are gravity recovery and atmospheric occultation. In the former, multipath errors that are not averaged over the period of the experiment will be directly mapped in the spherical harmonics; while in the latter, where instantaneous phase data is needed, multipath error will be mapped into the recovered atmospheric refractivity.

In this paper, the multipath effect on the GPS signal and its implications on orbit and ground positioning are examined. In order to do this, a multipath simulator, MUSTARD (MUltipath Simulator Taking into Account Reflection and Diffraction), has been developed. The following sections will describe the theoretical background and the application of the simulator.

Multipath Problem

If a satellite's signal propagates along a direct path to the receiver's antenna, the receiver can accurately determine the satellite range. However, the GPS signal can be easily reflected by other objects, thus resulting in possibly multiple secondary paths as shown in figure 1. These paths are always longer than the direct path, and are superimposed on the direct signal at the antenna with a different phase and amplitude. The signal wave-form's amplitude and phase can be significantly distorted by these secondary paths and thus can result in significant ranging errors.

The Purpose of the Multipath Simulator

The majority of the previous multipath research has focused on mitigating multipath errors. However, in the early design phase of an experiment, it would be desirable to predict hazardous environmental configuration that can cause severe multipath. With this information, we may attempt to modify the structural configuration if possible, or recommend the best antenna type, location, and orientation within the given configuration. In order to accomplish this, a multipath simulator, MUSTARD, has been developed at the Jet Propulsion Laboratory (JPL).

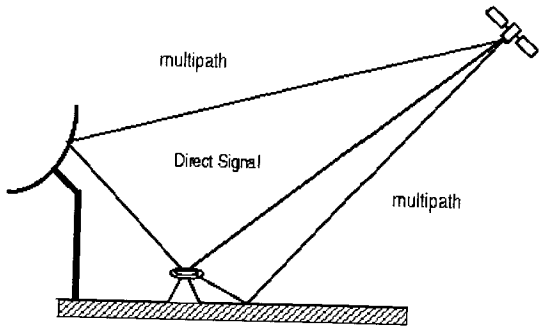

Figure 1: A multipath generating environment

In essence, the simulator traces the signal as it is transmitted by the GPS satellite to a user's receiver accounting for all possible paths the signal can take by reflecting or diffracting from the surrounding surfaces. In order to account for reflection and diffraction, the Geometrical Theory of Diffraction (GTD) is used (Hansen 1981; James 1980).

This sets a lower limit of a few wavelengths on the size of the reflecting objects. (In the case of GPS, the wavelengths are 19.0 cm and 24.4 cm at L1 and L2 frequencies, respectively.) The multipath signals are then added to the direct signal after accounting for the gain of the receiving antenna. The receiver's tracking loop is then simulated and then range and phase multipath error are estimated. This is done for both L1 and L2 frequencies that the GPS operates on.

This multipath simulator gives a realistic estimate of the error introduced by multipath, and helps to find a means of minimizing the effect of multipath. For precise orbit determination, for example, it provides a quantitative estimate of multipath errors and, thus, can be used for testing different ways of processing simulated observables containing multipath errors.

GPS SIGNAL STRUCTURE AND OBSERVABLES

GPS Signal Structure

The GPS transmits two RCP signals at L-band frequencies: L1 at 1575.42 MHz and L2 at 1227.6 MHz. The L2 signal and the in-phase component of the L1 signal are modulated by pseudo-random precision code (P-code) at a frequency of 10.23 MHz; the quadrature component of L1 is modulated by a coarse acquisition (C/A) code at a frequency of 1.023 MHz. A properly equipped receiver will detect amplitude, pseudorange, and phase measurements for each of the C/A, L1 P-code (P1), and L2 P-code (P2) signals (Spilker 1980).

Because the characteristics of C/A and P1 multipath errors

are very similar, our discussion below is simplified by considering only one of the two signals. Differences between P1 and C/A multipath will be pointed out as they become significant. To that end it is convenient to model the transmitted P1 and P2 signals as the real part of

$$S_i(t_T) = \tilde{A}_i P(t_T) \exp\Big(j(\omega_i t_T + \phi_{Ti})\Big) \quad (1)$$

where

t_T = transmitter time
i = index for L1 and L2, respectively
$\tilde{A}_i$ = signal amplitude
P = PRN code
ω_i = $2\pi f_i$, where f_i is the transmitted freq.
ϕ_{Ti} = transmitter bias between carrier and P-code

The equation does not show the Y (encrypted) code, the C/A component, or the data modulation at 50 *bps*. Note that the transmitter oscillator drift term is included in t_T.

GPS Observables

Due to the dispersive nature of the ionosphere, the L1 and L2 signals travels at two different velocities. Moreover, the group and phase velocities are different for each frequency. Therefore, we can write the received signal as:

$$R_i(t_R) = A_i P(t_R - \tau_i^g) \exp\Big(j\omega_i(t_R - \tau_i^p) + \phi_{Ri}\Big) \quad (2)$$

where

t_R = receiver time
i = the index for L1 and L2, respectively
A_i = the received signal amplitude
τ_i^g = pseudorange
τ_i^p = τ_i^g + differential ionospheric effect on phase
ϕ_{Ri} = ϕ_{Ti} + bias between carrier and P-code

Note that t_R includes the receiver oscillator drift term. Both τ_i^g and τ_i^p include the transmitter and receiver clock biases. A single GPS measurement consists of four observables: two phase measurements for the L1 and L2 frequencies, $\Phi_i = -\omega_i \tau_i^p + \phi_{Ri}$, with an unknown bias, and two pseudorange measurements, $P_i = c\,\tau_i^g$. By ignoring terms of order $1/f_i^3$ or higher, these observables can be written in units of distance as:

$$L_1 \equiv -c\frac{\Phi_1}{2\pi f_1} = \rho + n_1\lambda_1 - \frac{q}{f_1^2} + M_{L1} \quad (3)$$

$$L_2 \equiv -c\frac{\Phi_2}{2\pi f_2} = \rho + n_2\lambda_2 - \frac{q}{f_2^2} + M_{L2} \quad (4)$$

$$P_1 = \rho + \frac{q}{f_1^2} + M_{P1} \quad (5)$$

$$P_2 = \rho + \frac{q}{f_1^2} + M_{P2} \quad (6)$$

where ρ is the non-dispersive delay including the geometric delay, tropospheric delay, clock biases, and any other delay that effects all observables similarly; q is a parameter that is proportional to the total electron content (TEC), which is the integrated electron density between the transmitter and the receiver. Other parameters are:

c = the speed of light
λ_i = the wavelength for L1 and L2
n_i = unknown integer of cycles
q/f_i^2 = ionospheric group delay and phase advance
M_{Li} = the carrier multipath in range
M_{Pi} = the code multipath in range

Terms that are part of the observables but not included the equations 3–6 are data noise, phase center variation, higher order ionospheric terms, and a "wind-up" transmitter-receiver geometry dependent term (Wu et al. 1993). These terms will be assumed to be negligible, or they can be modeled and subtracted out.

Of importance to the subsequent analysis are the ionospheric free linear combinations:

$$\left(\frac{f_1^2}{f_1^2 - f_2^2}\right)P_1 - \left(\frac{f_2^2}{f_1^2 - f_2^2}\right)P_2 = \rho + \left(\frac{f_1^2}{f_1^2 - f_2^2}\right)M_{P1} - \left(\frac{f_2^2}{f_1^2 - f_2^2}\right)M_{P2} \quad (7)$$

$$\left(\frac{f_1^2}{f_1^2 - f_2^2}\right)L_1 - \left(\frac{f_2^2}{f_1^2 - f_2^2}\right)L_2 = \rho + \frac{f_1^2 M_{L1} - f_2^2 M_{L2}}{f_1^2 - f_2^2} + \frac{f_1^2 n_1\lambda_1 - f_2^2 n_2\lambda_2}{f_1^2 - f_2^2} \quad (8)$$

and the P-code multipath linear combinations:

$$P_1 - \left(\frac{f_1^2 + f_2^2}{f_1^2 - f_2^2}\right)L_1 + \left(\frac{2f_2^2}{f_1^2 - f_2^2}\right)L_2 = M_{P1} + C_1 \quad (9)$$

$$P_2 - \left(\frac{2f_1^2}{f_1^2 - f_2^2}\right)L_1 + \left(\frac{f_1^2 + f_2^2}{f_1^2 - f_2^2}\right)L_2 = M_{P2} + C_2 \quad (10)$$

where C_1 and C_2 are biases.

In equations 7 and 8, the ionospheric term is removed and one is left with the pseudorange or biased phase plus a linear combination of L1 and L2 multipath. For the GPS $f1$ and $f2$ frequencies, the coefficients multiplying P1 and P2 in equation 7 are $2.54\cdots$ and $-1.54\cdots$, respectively. This implies that, if P1 and P2 multipath errors are about equal but uncorrelated, the multipath peak-to-peak amplitude is magnified by about a factor of 3 to that of either P1 and P2 alone. A similar analysis applies for the phase linear combination of equation 8.

In the last two linear combinations, the range, clock, and ionospheric terms are removed from the observables, and one

is left mainly with the multipath terms of P1 and P2 plus biases. The biases correspond to fixed numbers over an entire track for a give transmitter and receiver pair. In obtaining equations 9 and 10, we also ignore the carrier phase multipath, since it is generally two order of magnitude smaller than the P-code multipath.

MULTIPATH EFFECT ON THE GPS OBSERVABLES

In order to understand the effects of multipath in any given environment, we need to understand how the PRN ranging receivers operate and how multipath distortion results in ranging errors. The receiver's response to multipath can be parameterized by signal amplitude, time delay, phase, and phase rate. Note that all of the parameters are relative to the direct GPS signal. For the following discussion, a stable multipath is assumed and thus the relative phase rate is assumed to be zero.

Carrier Phase Multipath

In the presence of multipath signals such as depicted in figure 1, the total received signal is the superposition of the direct (equation 2) and delayed replicas of the direct. Concentrating on the carrier and ignoring the P-code modulation, we can write the total received signal as (dropping the subscripts in equation 2):

$$R(t) = Ae^{j(\omega t - \omega\tau + \phi)} + \sum_{k=1}^{N} A_k e^{j(\omega t - \omega\tau_k + \phi + \phi_k)} \quad (11)$$

where the sum is over all possible multipath signals, and A and A_k are the amplitudes of the direct signal and the multipath signal from point k, respectively. The corresponding time delays are τ and τ_k; ϕ_k is the additional phase introduced by the multipath signal coming from point k. In order to find the phase error introduced by the extra paths, we factor out the term $Ae^{j(\omega t - \omega\tau + \phi)}$, then equation 11 can be written as:

$$R(t) = Ae^{j(\omega t - \omega\tau + \phi)}\left(1 + \sum_{k=1}^{N} \frac{A_k}{A} e^{j(\omega\Delta\tau_k + \phi_k)}\right) \quad (12)$$

where $\Delta\tau_k$ is the extra travel time of the multipath signal from point k. Therefore, an extra phase error is given by:

$$\delta\phi = \arctan\left(\frac{\sum_{k=1}^{N} \frac{A_k}{A}\sin(\omega\Delta\tau_k + \phi_k)}{1 + \sum_{k=1}^{N} \frac{A_k}{A}\cos(\omega\Delta\tau_k + \phi_k)}\right) \quad (13)$$

In the limit when $A_k/A \ll 1$ for all k's, we can expand equation 13 as:

$$\delta\phi = \sum_{k=1}^{N} \frac{A_k}{A}\sin(\omega\Delta\tau_k + \phi_k) \quad (14)$$

Code Multipath

In tracking the transmitted GPS code signal, the received signal is correlated with a locally generated replica of the code. The receiver computes the correlation function between the received signal and the internally generated signal at three different modeled delays called "prompt", "early", and "late". The "early" and "late" delays are different from the "prompt" delay by a receiver sampling interval $+S$ and $-S$ ns, respectively. The receiver effectively fits a equilateral triangle with base length of two chip period, $2T$, on these three points and declares the location of the peak to be the true delay. In the absence of any multipath, the correlation between the received signal and the receiver generated code can be approximated by a equilateral triangle with a peak value of A and a phase $\exp[i(\phi_m - \phi)]$, where ϕ_m are the modeled phase. In the presence of a single multipath signal with an additional time delay of $\Delta\tau_1$, amplitude of A_1, and phase shift ϕ_1, the correlation function can be modeled as the sum of the two triangles corresponding to the direct and the multipath signal. The presence of multipath signals corrupt the triangular shape. Below we derive the formulation of the pseudorange measurement error for a given multipath amplitude, delay, and phase shift. That formulation is different depending on the sampling interval being larger or smaller than half a chip period, and ignores the effects of finite bandwidth on the shape of the correlation function.

Wide sampling interval

In the case of the sampling intervals longer than half of the chip length ($S > T/2$), the resulting error in the code measurement, $\Delta\tau_g$, induced by the presence of a single multipath is given by one of the following formulas (Young et al. 1988):

Region 1 which applies when $\Delta\tau_1 < T - S + \Delta\tau^g$:

$$\Delta\tau^g = \frac{\Delta\tau_1 \frac{A_1}{A}\cos(\omega\Delta\tau_1 + \phi_1)}{1 + \frac{A_1}{A}\cos(\omega\Delta\tau_1 + \phi_1)} \quad (15)$$

Region 2 which applies when $T - S + \Delta\tau^g < \Delta\tau_1 < S + \Delta\tau^g$:

$$\Delta\tau^g = \frac{(T - S + \Delta\tau_1)\frac{A_1}{A}\cos(\omega\Delta\tau_1 + \phi_1)}{2 + \frac{A_1}{A}\cos(\omega\Delta\tau_1 + \phi_1)} \quad (16)$$

Region 3 which applies when $S + \Delta\tau^g < \Delta\tau_1 < T + S + \Delta\tau^g$:

$$\Delta\tau^g = \frac{(T + S - \Delta\tau_1)\frac{A_1}{A}\cos(\omega\Delta\tau_1 + \phi_1)}{2 - \frac{A_1}{A}\cos(\omega\Delta\tau_1 + \phi_1)} \quad (17)$$

Region 4 which applies when $\Delta\tau_1 > T + S$:

$$\Delta\tau^g = 0 \quad (18)$$

Figure 2 shows the P1 pseudorange multipath induced error $\Delta\tau^g$ as a function of the multipath delay $\Delta\tau_1$. Values of

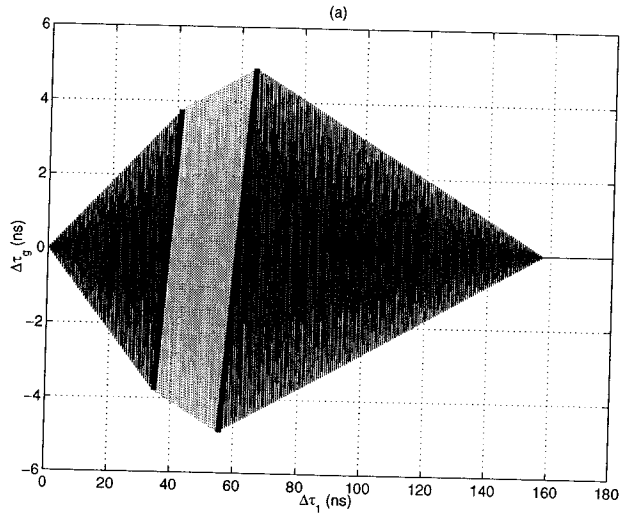

Figure 2: The P1 code tracking error when $S > T/2$ as a function of a single multipath source with multipath delay of $\Delta\tau_1$. The relative multipath amplitude is assumed constant ($A_1/A = 0.1$), values of $T = 98\,ns$, $S = 60\,ns$, and $\phi_1 = 0$ are used. There are four distinct regions corresponding to equations 15–18. Regions 1–3 are separated by thick solid lines for clarity.

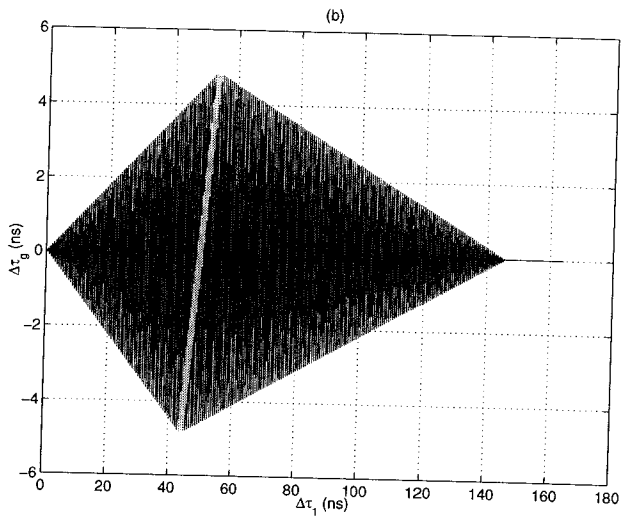

Figure 3: The P1 code tracking error when $S < T/2$ as a function of $\Delta\tau_1$. Values of $A_1/A = 0.1$, $T = 98\,ns$, $S = 48\,ns$, and $\phi_1 = 0$ are used. The four distinct regions corresponding to equations 19–22.

$T = 98\ ns$, $S = 60\ ns$, and $A_1/A = 0.1$ are used. The envelope of the multipath error can be readily seen in the figure. The upper envelope corresponds to the multipath error which is in phase with the direct signal, while the lower envelope corresponds to the out-of-phase case. The three different slopes of the upper or lower envelopes correspond to the three different regimes of equations 15–17 and they are separated by two thick black lines in the figure for clarity. The asymmetry of the envelope is amplified for higher values of A_1/A.

The C/A pseudorange multipath induced error is also given by equations 15–18 as long as $S > T/2$, where T is a C/A code chip period. This causes the different regimes of equations 15–17 to trigger at different values of $\Delta\tau_1$. Specifically, the C/A code multipath induced error can grow to 10 times larger than the P-code and does not vanish until $\Delta\tau_1 > T + S$. On the other hand, for various reasons it is the region of small multipath delays that is most important for most GPS applications, and in this region the P1 and C/A multipath errors are the same.

Narrow sampling interval

When $S < T/2$, $\Delta\tau_g$ is given by one of the following formulas:

Region 1 which applies when $\Delta\tau_1 < S + \Delta\tau^g$:

$$\Delta\tau^g = \frac{\Delta\tau_1 \frac{A_1}{A}\cos(\omega\Delta\tau_1 + \phi_1)}{1 + \frac{A_1}{A}\cos(\omega\Delta\tau_1 + \phi_1)} \tag{19}$$

Region 2 which applies when $S + \Delta\tau^g < \Delta\tau_1 < T - S + \Delta\tau^g$:

$$\Delta\tau^g = S\frac{A_1}{A}\cos(\omega\Delta\tau_1 + \phi_1) \tag{20}$$

Region 3 which applies when $T - S + \Delta\tau^g < \Delta\tau_1 < T + S$:

$$\Delta\tau^g = \frac{(T + S - \Delta\tau_1)\frac{A_1}{A}\cos(\omega\Delta\tau_1 + \phi_1)}{2 - \frac{A_1}{A}\cos(\omega\Delta\tau_1 + \phi_1)} \tag{21}$$

Region 4 which applies when $\Delta\tau_1 > T + S$:

$$\Delta\tau^g = 0 \tag{22}$$

Note that equation 20 is not a function of T, and the boundary values of each region are different.

Figure 3 shows the P1 pseudorange multipath induced error $\Delta\tau^g$ for the $S < T/2$ case. Values of $T = 98\ ns$, $S = 48\ ns$, and $A_1/A = 0.1$ are used. A main distinction between the narrow and wide sampling interval is that in the former, the error exhibit a constant peak value in region 2. This becomes clear as we consider the corresponding figure for the C/A code. Figure 4 was generated using $T = 980\ ns$, $S = 48\ ns$, and $A_1/A = 0.1$. Note that the C/A code multipath induced error exhibits a very wide region 2 and does not vanish until $T + S = 1028\ ns$.

Multipath induced bias

When $A_1/A \ll 1$, region 1 translate to $\Delta\tau_1 < T - S$ (wide sampling) and to $\Delta\tau_1 < S$ (narrow sampling). For $S = 60\,ns$ (wide sampling) and $48\,ns$ (narrow sampling) this translate

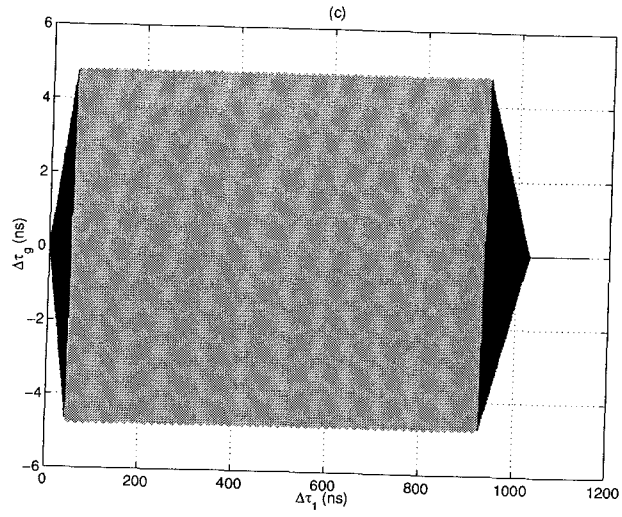

Figure 4: The C/A code tracking error when $S < T/2$ as a function of $\Delta\tau_1$. Values of $A_1/A = 0.5$, $T = 980\,ns$, $S = 48\,ns$, and $\phi_1 = 0$ are used. The four distinct regions corresponding to equations 19–22.

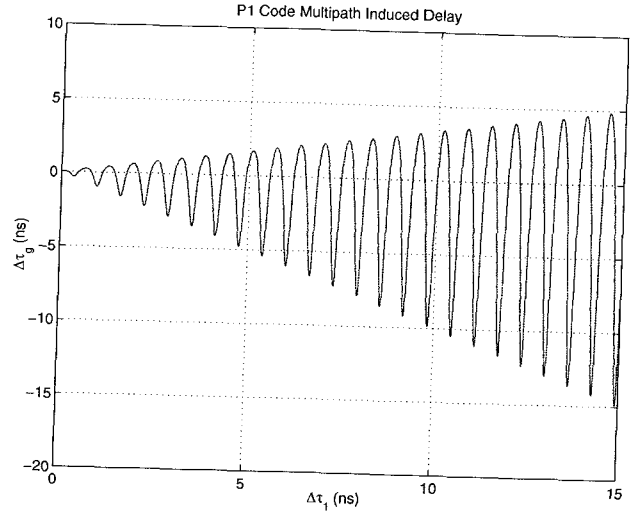

Figure 5: Detailed view of region 1 of the P1 code tracking errors showing the asymmetric and biased oscillation due to the carrier signal. Values of $A_1/A = 0.5$, $T = 98\,ns$, $S = 48\,ns$, and $\phi_1 = 0$ are used.

to $c\,\Delta\tau_g < 11\,m$ and $c\,\Delta\tau_g < 14\,m$, respectively. These are above the multipath distance that we will deal with in our discussion later. Therefore, equation 15 (which is identical to 19) becomes valid for P1, P2, and C/A code.

The effect of the denominator in equation 15 is to change the amplitude asymmetrically for in-phase and out-of-phase multipath. This will introduce a negative bias when integrating over a complete cycle. This implies that multipath does not average out and could cause a significant bias when A_1/A is not small. Figure 5 shows a magnified version of region 1 for $A_1/A = 0.5$.

When $A_1/A \ll 1$, $\Delta\tau_g$ varies more or less sinusoidally as a function of the multipath delay, and the multipath bias becomes second-order in A_1/A. For small ratios of A_1/A, the multipath bias is approximately, $-1/2\,\Delta\tau_1(A_1/A)^2$.

Setting aside the amplitude scaling effect of the denominator in equation 15, we can concentrate on the numerator part of the equation and use the approximation

$$\Delta\tau^g \simeq \Delta\tau_1 \frac{A_1}{A}\cos(\omega\Delta\tau_1 + \phi_1) \qquad (23)$$

In order to understand more the implication of equation 23, we consider an example of a plane reflector as shown in figure 6. In this example, we have

$$\Delta\tau_1 = \frac{L_m}{c} = \frac{2L\sin\theta}{c} \qquad (24)$$

where L_m is the extra traveled distance due to multipath, L is the antenna height, and θ is the satellite elevation angle. Let $\theta = \omega_s t$, where ω_s is the orbital angular frequency of the

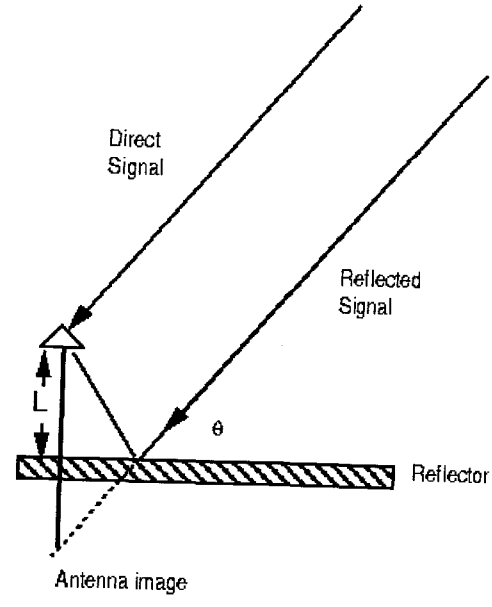

Figure 6: The geometric configuration of an antenna positioned on a plan reflector, the direct and the reflected signal.

transmitting satellite as seen by the receiver. By substituting equation 24 in equation 23, we get:

$$\Delta P = 2L\sin(\omega_s t)\frac{A_1}{A}\cos\Big(4\pi\frac{L}{\lambda}\sin(\omega_s t) + \phi_1\Big) \quad (25)$$

where λ is wavelength of the carrier signal, and ΔP is $c\,\Delta\tau^g$. Based on equation 25, ΔP is governed by two oscillations: a slow one, ω_s, and a fast one governed by the *cos* term in equation 25. In order to quantify this fast oscillation, we expand the *sin* term around a reference angle ϕ_r as follows:

$$\sin(\omega_s t) = \sin(\phi_r) + (\omega_s t - \phi_r)\cos(\phi_r) \quad (26)$$

Using this approximation in equation 25, dropping constant phase terms, and keeping the time varying terms, we can get:

$$\Delta P = 2L\sin(\omega_s t)\frac{A_1}{A}\cos\Big(4\pi\frac{L}{\lambda}\cos(\phi_r)\omega_s t\Big) \quad (27)$$

Since $\omega_s = 2\pi/\tau_s$ where τ_s is the orbital period of the satellite, we can derive from equation 27 that the period for high frequency multipath oscillation is

$$\tau_1 = \frac{\tau_s}{4\pi\frac{L}{\lambda}\cos(\phi_r)} \quad (28)$$

As is evident from equation 28, the multipath oscillation period is proportional to the wavelength. This implies that P1 multipath is oscillating faster than P2.

SIMULATOR DESCRIPTION

A multipath simulator, MUSTARD, for analyzing the effects of GPS signal multipath was developed at JPL. This software uses a ray-tracing technique to determine the different paths that a GPS transmitted signal can take. The capabilities of the simulator include:

GPS signals: handles both L1 and L2 frequencies; simulates RCP and LCP reflected and diffracted signals; estimates the multipath delay in the pseudorange and phase measurements

Reflection modeling: uses the Geometrical Theory of Diffraction (GTD) to model signal reflection and diffraction from surfaces, edges, and corners; handles simultaneous reflections from many surfaces

Antenna and receiver: simulates the antenna gain pattern for RCP and LCP signals for L1 and L2; simulates a receiver's operations on incoming signals which produce output observables

Surrounding environment modeling: models flat surfaces of arbitrary shape, spheres or sections of spheres (antenna dishes, inside and outside), cylinders or sections of cylinders, conducting or dielectric surfaces

Geometry: models the motion of the GPS transmitters and receivers and their attitudes to derive time series of the multipath error

By analyzing the real GPS data at the Ovro site, Hajj (1989) showed that MUSTARD could simulate very reasonable multipath errors. Modeling the multipath effects can help determine optimum configurations of the surrounding environment as well as predict the errors that the system will experience. Thus, this software is especially useful in the design phase of a flight mission or ground experiments to quantify the effect of the signal multipath for different GPS antenna types and locations.

Multipath Modeling

The simulator uses simplified model of the real multipath environment where the geometry of the reflecting structures, the transmitting and the receiving antennas is approximated. The multipath environment is generally modeled as a finite number of surfaces whose dimensions, relative locations, and orientations, as well as their electromagnetic properties are specified.

In modeling the reflection and diffraction from each surface, the Geometric Theory of Diffraction (GTD) is used. The details of this theory is worked out for many types of surfaces with different shapes and electromagnetic properties (Hansen 1981; James 1980). Below we present some simple examples of how MUSTARD ray-trace a signal as it reflects from a flat surface with an arbitrary shape and from an edge.

Reflection From A Flat Surface

When considering specular reflection from flat surfaces, the problem can be simply stated as follows: In a specified reference frame, given a transmitter at location $\mathbf{T}$, a receiver at location $\mathbf{R}$, a flat surface with a defined point on the surface at $\mathbf{V}$, and a unit vector $\mathbf{n}$ normal to the surface as shown in figure 7; we want to find the point of reflection inside the surface, $\mathbf{S}$, if any. To do this, we extend the finite surface to an infinite one, and given the latter, we can find the mirror image of the receiver $\mathbf{R_{image}}$ given by:

$$\mathbf{R_{image}} = \mathbf{R} - \mathbf{2n}\cdot\mathbf{R} \quad (29)$$

We can draw a line connecting the image point, $\mathbf{R_{image}}$, and the transmitter. Then, the reflection point on the infinite surface is the intersection point of the line with the infinite plane. If $\mathbf{S}$ is defined as the solution vector of the reflection point, it should satisfy both the infinite surface equation

$$(\mathbf{S} - \mathbf{V})\cdot\mathbf{n} = \mathbf{0} \quad (30)$$

and the line equation connecting $\mathbf{T}$ and $\mathbf{R_{image}}$

$$\mathbf{S} = \mathbf{T} + t\,(\mathbf{R_{image}} - \mathbf{T}) \quad (31)$$

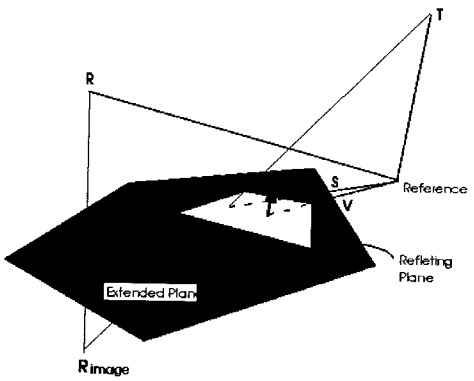

Figure 7: A depiction of specular reflection from a flat surface corresponding to the mathematical description of section .

where t is a parameter of a value from 0 to 1. The solution of the equations 30 and 31 is

$$\mathbf{S} = \mathbf{T} + \frac{\mathbf{n}\cdot\mathbf{V} - \mathbf{n}\cdot\mathbf{T}}{\mathbf{n}\cdot(\mathbf{R_{image}} - \mathbf{T})}\left(\mathbf{R_{image}} - \mathbf{T}\right) \qquad (32)$$

The corresponding extra path length, L_{mS}, due to specular reflection is then

$$L_{mS} = |\mathbf{T} - \mathbf{S}| + |\mathbf{R} - \mathbf{S}| - |\mathbf{T} - \mathbf{R}| \qquad (33)$$

Once the reflection point is determined on the infinite plane, we need to check whether it lies inside or outside of the finite surface. For the case of a polygon, this is best done by drawing a semi-infinite line in the reflection plane, originating at $\mathbf{S}$ and extending to infinity in any direction. If the line intersects the edges of the polygon zero or even number of times, then $\mathbf{S}$ must be outside of the polygon; otherwise, it is inside it. The amplitude, phase, and polarization of the reflected signal is based on the properties of the surface as well as the incident angle, and is determined by matching the boundary conditions at the surface (Heald and Marion 1995).

Once the point of reflection, $\mathbf{S}$, is found, the multipath delay due to specular reflection can be computed. For example, consider a simple semi-infinite plane, where a GPS antenna is located at height L from the surface and at distance d from the edge of the plane as shown in figure 8. Then the delay of the specularly reflected signal with respect to the direct is given by:

$$L_{mS} = 2L\sin\theta \qquad (34)$$

where θ is the GPS elevation angle from the surface plane. Assuming the surface to be a perfect conductor, then the specularly reflected signal is completely left-hand circularly polarized with the same power as the direct. It is important to

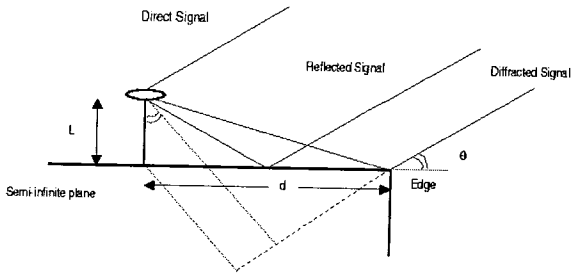

Figure 8: A depiction of reflection and edge diffraction corresponding to equations 34 and 35.

note that the received signal strengths differ due to the difference in RCP antenna gain toward the GPS satellite and LCP gain toward the reflecting surface. Given the multipath delay L_{mS}, the multipath code range error can be computed by using either equation 15 or 19.

Diffraction From An Edge

When an RCP signal diffracts from an edge, it is generally composed of both LCP and RCP signals. The power contained in each of these components depends on the direction of the incident and diffracted angles and is generally inversely proportional to the distance of the diffracting edge to the antenna. For example, considering the same plane in figure 8, the delay of the edge diffracted signal, L_{mD}, with respect to the direct is given by:

$$L_{mD} = \sqrt{L^2 + d^2} - d\cos\theta + L\sin\theta \qquad (35)$$

With this multipath delay, the multipath code range error can be computed by using either equation 15 or 19. The effects of the edge on the polarization and the power of the reflected signal are well characterized by (Kouyoumjian and Pathak 1974).

Antenna Gain Pattern

Partial multipath signal rejection can be achieved by properly shaping the antenna gain pattern and polarization. Usually, the antenna gain pattern is shaped in such a way that overall gain, and particularly LCP gain, drop off quickly at low elevation angles so that reflected signals received at very low and negative elevations are significantly attenuated. Signals from lower elevations are more likely to be reflected from a nearby object.

Figure 9 shows an example of a GPS receiving antenna gain pattern corresponding to a Dorne-Margoline (D-M) antenna. The figure depicts the antenna gain as function of boresight angle for a specific azimuthal angle and for L1, L2, RCP, and

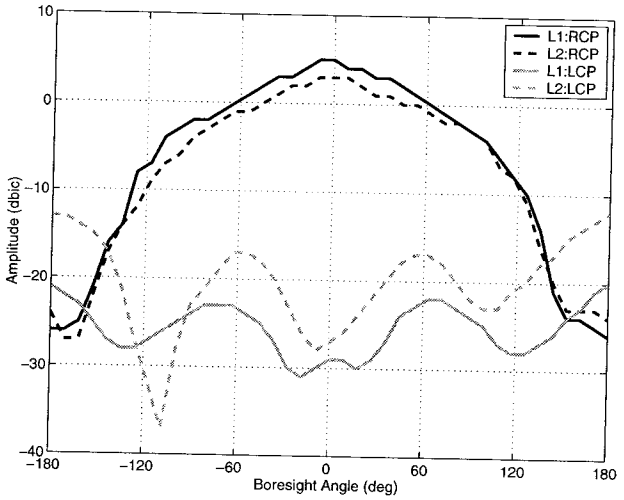

Figure 9: The gain pattern of a Dorne-Margoline antenna. Note that 0 deg corresponds to the antenna boresight direction.

LCP. Note that, for example, for satellite at 30° elevation, the L1 multipath rejection is given by the RCP gain toward the satellite (0 $dBic$) minus the LCP gain toward the reflection at $-30°$ elevation (-27 $dBic$) for a rejection factor of 27 dB. The multipath simulator can accommodate any particular antenna gain pattern.

APPLICATION OF THE MULTIPATH SIMULATOR

By using the GPS multipath simulator, MUSTARD, we can do various tests to reduce the multipath effects. For example, we can try to find the optimal GPS antenna location and attitude, select the beset antenna gain pattern, or we can try different data analysis schemes to improve the overall solution from the GPS data.

MUSTARD has been used in the early design phase of the TOPEX satellite mission to quantify the effect of signal multipath for different GPS antenna positions, antenna gains, and data analysis techniques. Hajj (1989) showed that the multipath effect can be mitigated up to about 20 db lower than the direct signal by properly adjusting the on-board GPS antenna height. It has also been used for the assessment of the GPS signal multipath on the SIR-C/X-SAR free flyer environment for the satellite attitude determination using GPS, and showed that the GPS can be used to meet the attitude requirement on SIR-C/X-SAR (Hajj and Ceva 1994).

Recently, MUSTARD was used to study the Primary Atomic Reference Clock in Space (PARCS) experiment. The purpose of PARCS is demonstrating state-of-the-art atomic clock performance in space. The microgravity environment of space allows significant improvements in clock performance over ground-based clocks, thus opening up potential ultra-precise reference clocks in space. The demonstration will be carried out on the International Space Station (ISS) in year 2005. It will carry a laser cooled precision clock driven by a hydrogen maser (Wu and Byun 2001). GPS measurements accurately determine the ISS orbit. The orbit is needed for the precise determination of the ISS velocity and position in the Earth's gravitational field, in order to correct for the effects of special and general relativity on the PARCS clock behavior. Since the on-board GPS receiver will operate coherently with the PARCS clock, it will also be used to measure the offset of the PARCS clock from various stable ground clocks connected to their own GPS receivers. The GPS antenna will be located at the Japanese Experiment Module (JEM) where the multipath interference is severe. The application of MUSTARD to the PARCS experiment is described in the following subsections.

Table 1: The orbit elements of ISS on 1998 09 22, 00:00:00 UTC

Semi-major axis	6785 km
Eccentricity	0.02
Inclination	51.6°
Argument of periapsis	90°
Right ascension	330°
Mean anomaly	0°

Spacecraft Modeling

ISS is modeled with a circular orbit at 407 km altitude. The orbit elements of ISS at an epoch of 1998:09:22 00:00:00 UTC are as shown in table 1. This orbit was integrated forward over one day and used as the nominal ISS orbit. For the attitude of ISS, we assumed that the spacecraft body-fixed z-axis always points toward Earth center, the y-axis is normal to the orbit plane but opposite to orbit angular momentum vector, and the x-axis completes the right-handed system. The precise GPS orbits and clocks determined by Flinn network on the same day were used (Jefferson et al. 1999). L1, L2, and ionospheric-free GPS pseudorange and carrier phase data were simulated between the ISS and all visible GPS satellites at 5 minute intervals over one day.

For modeling of the environment of JEM where the flight GPS receiver will be located, simplified models of three major multipath sources were considered as shown in figure 10. They are stationary objects close to GPS antenna and consist of Pressurized Module (PM), Exposed Facility (EF), and Experiment Logistics Module-Exposed Section (ELM-ES).

Assessing The Multipath Error

For our study the D-M antenna pattern shown in figure 9 was used, assuming azimuthal symmetry. The antenna is assumed to be placed at the center of the EF, but one meter above its

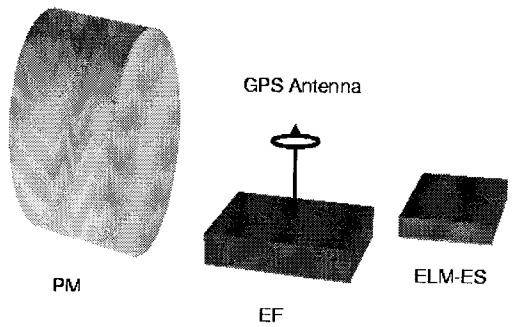

Figure 10: The environmental modeling of reflecting surfaces of JEM showing Pressurized Module (PM), Exposed Facility (EF), and Experiment Logistic Module-Exposed Section (ELM-ES)

top surface. We assume the on-board GPS receiver tracks all visible GPS satellites, with an antenna elevation cutoff at zero degrees.

Figure 11 shows relative strengths of direct and reflected signals at L1 and L2 frequencies from each modeled surface. The horizontal axis of each plot denotes the angle of the GPS satellites with respect to the antenna boresight. The dark circle marks denote the direct signal strength while the light plus marks denote the reflected signal strength. In constructing these plots only specular reflection is considered which explains the gaps at certain boresight angles. These gaps imply that no specular reflection is possible when the GPS satellite is at that boresight angle range. From this figure, we can see that the major multipath contributors are EF and PM but not ELM. According to figure 9, the antenna has better multipath attenuation characteristics at L1 frequency (solid line) than at L2 (dotted line). Multipath attenuation is the separation between the RCP gain at the boresight angle (direct signal gain), and the LCP gain at 180°− boresight angle (reflected signal gain). This is also seen in figure 11.

Figure 12 shows the P1, P2, and PC pseudorange multipath from EF due to signal reflections only from all visible GPS satellites as a function of the GPS elevation angle. Plotting the multipath with respect to the elevation angle rather than time shows the geometric characteristics of the reflecting structure better. This can be beneficial in the early design phase of the spacecraft. The figure shows that multipath due to signal reflection from EF are mainly from the satellites at high elevation angles. This is contrary to the general notion, but is explained by examining figure 11 and equation 15. Figure 11 shows the ratio of direct to multipath gain is greater toward the antenna boresight. In addition, equation 15 shows the multipath error is proportional to the multipath additional

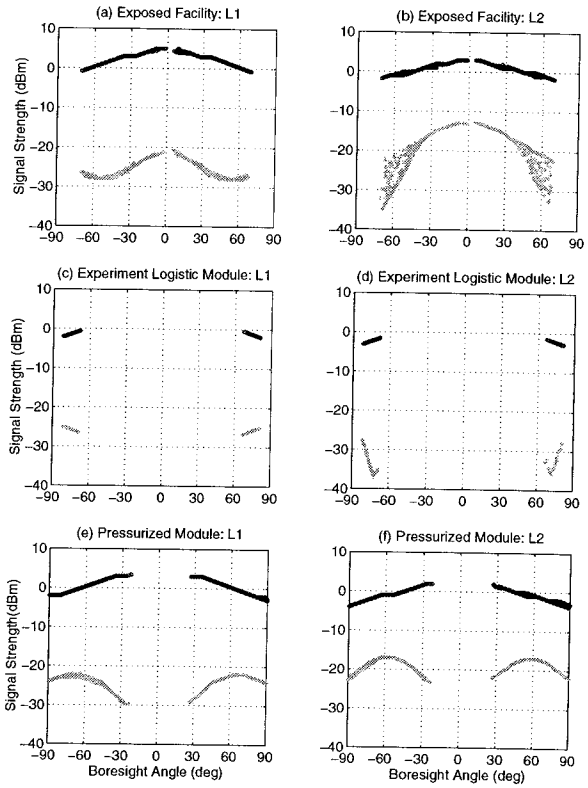

Figure 11: A comparison of the direct (dark color) and specular reflected (light color) signal strength for EF, ELM-ES, and PM structures

delay, which is $2L\sin(\theta)$ where θ is the GPS elevation angle, so is smaller at low elevation angles. Because of the worse L2-LCP antenna gain pattern relative to the L1-RCP (see figure 9), the P2 signal has larger multipath errors than P1. PC has the highest multipath effect due to the multiplicative coefficients in equation 7.

Figure 13 shows the P1, P2, and PC pseudorange multipath from EF due to both signal reflection and diffraction from all visible GPS satellites. Due to the small size of EF, the signal diffraction from the edge at low elevation can easily reach the antenna. By comparing figures 12 and 13, it can be seen that the major multipath contribution is from signal diffraction at low elevation angles, and from signal reflection at high elevation angles. Even though not shown, very similar characteristics for phase multipath can be seen but at 100 times smaller scale. Similar plots can be made for the P-code pseudorange multipaths due to reflection and diffraction from ELM and PM, respectively. As can be inferred from figure 11, ELM does not contribute much to the specular multipath error but has a significant contribution to multipath at all GPS elevations when diffraction is included. In the case of PM, a large portion of multipath errors are caused by the signals from the GPS satellites at very low elevation angles due to its vertical reflecting surface.

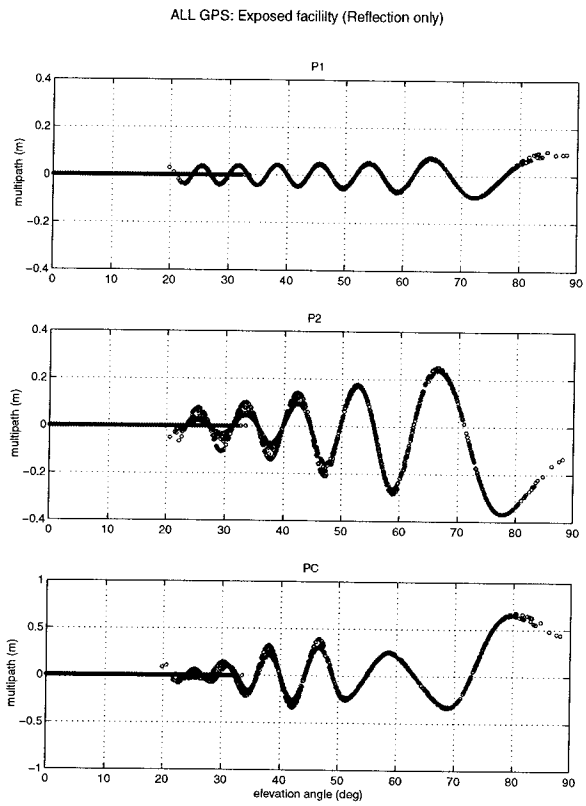

Figure 12: P-code multipath errors due to signal reflections from EF as a function of the GPS satellite elevation angle. Multiple values correspond to different GPS satellites.

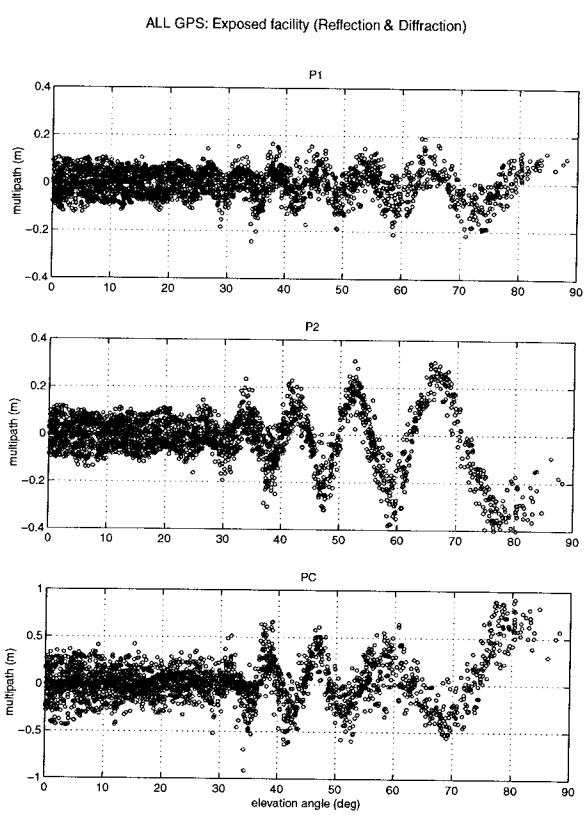

Figure 13: Same as figure 12 but diffraction included.

Table 2: The GPS antenna height effect on multipath error

antenna height	PC(m)	LC(m)
0.2 m	0.7970	0.0108
1 m	0.7137	0.0087
2 m	0.7139	0.0077
3 m	0.7066	0.0070
4 m	0.6759	0.0067

Finally, figure 14 shows the total P-code pseudorange multipath from all structures, and similar plot can be made for the total phase. Note that in figure 14 the horizontal axes are a time scale instead of GPS elevation angle. The root sum square value of multipath is 0.71 m for PC, and 0.87 cm for LC as shown in table 2.

Optimal Location Of The Antenna

The effects of multipath on GPS measurements will depend on the antenna location with respect to the reflecting surfaces. When changing the surrounding environment is not an option, a simple approach to reducing multipath is to find the best antenna location within a given environment.

Since the purpose of this article is to demonstrate the capability of MUSTARD, no extensive search for the best antenna location was performed. Instead, the antenna location was fixed at the center of EF, but its height was adjusted to illustrate the resulting multipath error variation. Table 2 shows the GPS antenna height effect on the multipath error. As the antenna height gets higher, the multipath errors are diminished. MUSTARD allows the user to choose a height which satisfies a given orbit accuracy requirement. It is probable that better results could be obtained with a more easily accommodated flush-mounted antenna using a more favorably shaped antenna gain pattern.

CONCLUSIONS

It is possible to investigate the multipath effect on the GPS signal by using a multipath simulator, MUSTARD, developed at JPL. In essence, this simulator trace the GPS signal as it is transmitted by the GPS satellite to a user's receiver accounting for all possible different paths due to specular reflection and diffraction from surrounding surfaces. In order to account for signal reflection and diffraction, the Geometrical Theory of Diffraction is used. The non-negligible multipath signals are added to the direct GPS signal. The simulator then ac-

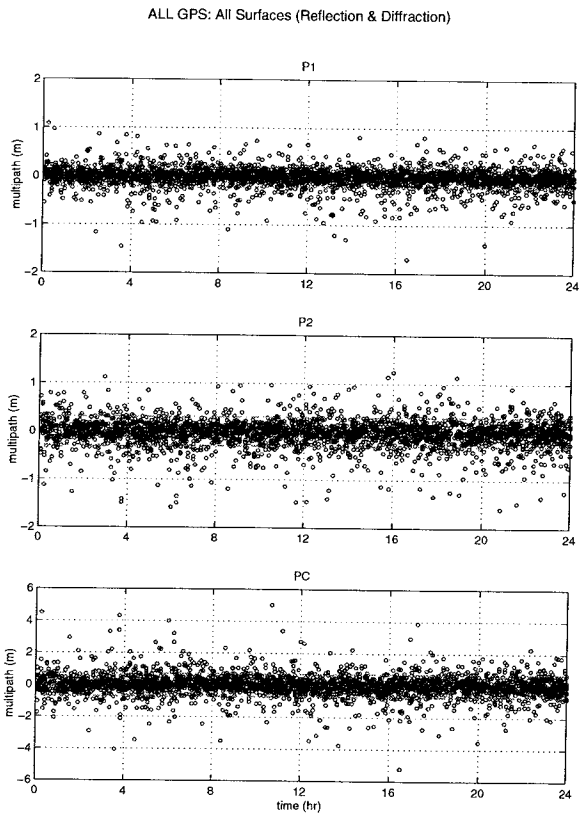

Figure 14: P-code multipath errors due to signal reflections and diffractions from all surfaces with respect to time

counts for the gain of the GPS antennas at L1, L2, RCP, and LCP, and the corresponding induced phase and range errors as measured by a delay-lock loop receiver are estimated.

The multipath simulator can be used in the initial design phase of an experiment to identify environmental configurations that can cause severe multipath. By using the simulator we can also assess the upper limits on the antenna backlobe gains, and be able to determine the ideal antenna location, height, and orientation to minimize the multipath error within a given environment.

Once the optimal geometric configuration is determined, MUSTARD can provide a realistic and quantitative estimate of multipath errors on GPS data. This in turn can provide a means of testing different ways of analyzing the data to reduce the solution errors from multipath. With a given environment, this simulator is a valuable tool to quantitatively assess the multipath effect on the GPS measurement.

ACKNOWLEDGMENTS

The research described in this article was carried out at the Jet Propulsion Laboratory, California Institute of Technology, under a contract with the National Aeronautics and Space Administration.

REFERENCES

Bassiri, S. and G. A. Hajj (1993). Higher-order ionospheric effects on the global positioning system observables and means of modeling them. *Manuscripta Geodaetica 18*, 280–289.

Hajj, G. and J. Ceva (1994, Aug). Preliminary assessment of the gps signal multipath on the SIR-C/X-SAR free-flyer. JPL Memorandum:335.8-94-008.

Hajj, G. A. (1989, Oct.10-11). The multipath simulator: A tool toward controlling multipath. In *Proceedings of the 2nd symposium on GPS applications in space*, Hanscom AFB, MA. Air Force, Geophysics Research Lab.

Hansen, R. C. (Ed.) (1981). *Geometric Theory of Diffraction*. IEEE Press selected reprint series. New York: IEEE Press.

Heald, M. A. and B. Marion, Jerry (1995). *Classical electromagnetic Radiation* (3rd ed.). Fort Worth: Saunders College Pub.

James, G. L. (1980). *Geometric theory of diffraction for electromagnetic waves* (Revised ed.), Volume 1 of *IEE Electromagnetic waves series*. Stevenage, UK: Peter Peregrinus Ltd.

Jefferson, D., Y. Bar-Sever, M. Heflin, M. Watkins, F. Webb, and J. Zumberge (1999, Nov). JPL IGS analysis center report, 1998. In K. Gowey, R. Neilan, and A. Moore (Eds.), *International GPS service for Geodynamics 1998 Technical Reports*, pp. 89–97. Pasadena, CA: Jet Propulsion Laboratory, California Institute of Technology.

Kouyoumjian, R. G. and P. Pathak (1974, Nov). A uniform geometrical theory of diffraction for an edge in a perfectly conducting surface. *Proc. IEEE 62*, 1448–1461.

Spilker, J. J. (1980). Signal structure and performance characteristics. In *Global Positioning System*, pp. 29–54. Washington, DC: The Institute of Navigation.

Wu, J. T., S. C. Wu, G. A. Hajj, W. I. Bertiger, and S. M. Lichten (1993). Effects of antenna orientation on GPS carrier phase. *Manuscripta Geodaetica 18*, 91–98.

Wu, S.-C. and S. Byun (2001, Sep). Frequency transfer in space with GPS measurements. In *Proceedings of the ION GPS-2001 14th International Technical Meeting of The Satellite Division of The Institute of Navigation*, Salt Lake City, UT. ION.

Young, L., T. Meehan, D. Spitzmesser, and J. Tranquilla (1988, Aug. 9-12). GPS antenna selection: Preliminary range and field test results. In *Proceedings of ANTEM 88*, Winnepeg, Manitoba, Canada.